ACS OMEGA

http://pubs.acs.org/journal/acsodf

Article

Numerical Simulation and Experimental Study for the Impact of In-Flow Nozzle on Spray Characteristics

Mahmoud Abd El-Aziz Mohamed,* Hesham El-Sayed Abdel Hameed, ElShenawy A. ElShenawy, Hafez Abdel Aal El-Salmawy, and Ramy Elsayed Shaltout

Cite This: *ACS Omega* 2021, 6, 33498−33510

Read Online

ACCESS | Metrics & More | Article Recommendations | Supporting Information

ABSTRACT: The impact of the in-flow characteristics inside the injection nozzle on atomization has been experimentally and computationally studied. Measurements are carried out using a transparent glass nozzle. Pulsed laser sheet with a synchronized charge-coupled device (CCD) camera and image processing, together with a particle image velocimetry (PIV) setup have been used as measuring techniques. Images and relevant image processing are used to visualize and quantify the rate of generation of cavitation bubbles inside the nozzle, the spray particle size distribution, and cone angle. Velocities inside and outside the injection nozzle are measured using PIV. The experimental investigation has been extended to include a wider range of the injection nozzle geometrical aspect ratios and working parameters. The computational model is a three-dimensional, two-phase, turbulent model to solve both the in- and out-nozzle flows. A novel coupling mathematical model is proposed for the definition of the probability density function of the issuing droplet size distribution, based on the in-flow developed conditions. A good agreement between both the experimental and computational results has been found under all conditions. According to both the experimental and computational results, it has been found that the onset of cavitation inside the injection nozzle, its location, collapse, and consequently the issuing spray configurations depend on the flow cavitation number, the nozzle geometrical characteristics, the liquid temperature, and the injection and back pressures. According to the quality of the obtained results from the model, it can be used to extend the study to cover a wider range of spray applications.

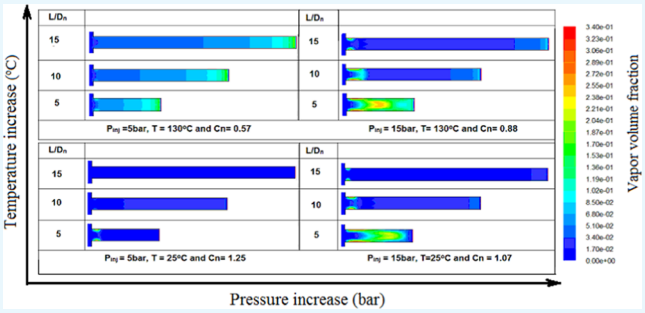

1. INTRODUCTION

Liquid atomization has many applications in combustion, industry, agriculture, and medicine. Achieving proper atomization is very much important to respond to the needs of applications.[1] This depends on both the atomized liquid properties and the atomization system design. Understanding, and consequently be able to model the atomization process, is an important step to fine control the atomization mechanism such that the requested atomization characteristics can be achieved.[2] One of the most widely used atomization techniques is the mechanical atomization, in which the liquid is pressurized against a fine nozzle.[3] Understanding this basic atomization process will help in further understanding the spray formation process.

A typical sequence of events that occur during spray development starts with injection, where an intact liquid column is issuing out of the injector nozzle.[4] Old theories[5] attributed atomization to the waves created in the issuing liquid jet as a result of the aerodynamic forces, and consequently, it is a function of jet velocity. Recent studies proved that the flow characteristics inside the injection nozzle influence the liquid jet and, in particular, the cavitation.[6] The hydrodynamic pressure drop of the working fluid is the main reason for the inception of this phenomenon, which is often called hydrodynamic cavitation.[7] Cavitation can be induced by both throttling effects and flow redirection, which are experienced inside the injector passage.[8] Furthermore, the studies revealed that the change in the convergent angle has significant effects on flow characteristics and the generation of cavitation.[9]

Hiroyasu[10] showed that liquid turbulence generated as a result of cavitation inside the injector nozzle plays an important role in atomization. He showed that even under a considerably high injection pressure, when cavitation does not take place inside the nozzle, the liquid jet does not atomize and the breakup length becomes longer. On the contrary, when cavitation takes place in the injection nozzle, atomization of

Received: August 9, 2021
Accepted: November 22, 2021
Published: November 30, 2021

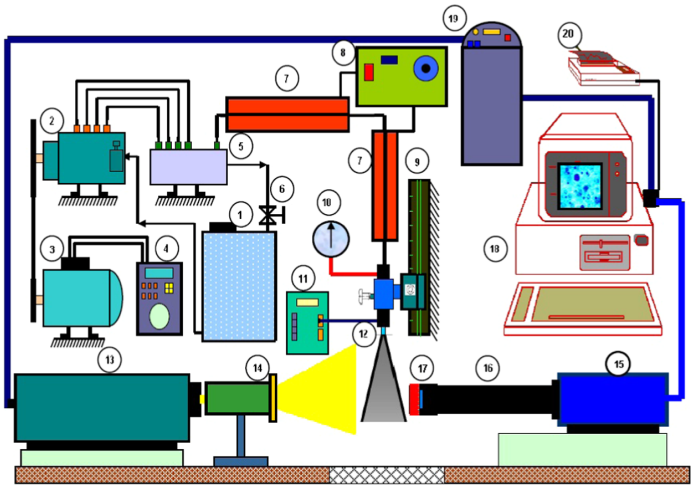

1 – Distilled water tank	8 – Temperature controller	15 – CCD Camera
2 – High pressure injection pump	9 – Traverse mechanism	16 – Extension tube
3 – AC motor (1 Hp)	10 – Bourdon-tube pressure gauge	17 – Camera focus lenses
4 – Inverter	11 – Temperature readout	18 – Synchronizer
5 – Accumulator	12 – Single hole nozzle injector	19 – Laser power supply
6 – Return valve	13 – Double pulse Nd:YAG laser	20 – Printer
7 – Pipe line heater	14 – Fluorescence plate	15 – CCD Camera

Figure 1. Schematic diagram of the experimental setup.

the liquid jet is considerably increased, and breakup length becomes shorter. He concluded that, at the beginning of the atomization regime, there is a bubbly liquid jet formed due to cavitation inside the injector nozzle. This regime is also called churning flow.[11] Due to cavitation, liquid turbulence, aerodynamic forces, velocity profile, and fuel pressure oscillation, the intact column breaks up into droplets.[12] Nurick[13] studied the cavitation phenomenon in the flow in an aperture. He observed that cavitation inside the nozzle could control the quality of mixture formation. He mapped the cavitation number, considering all of the dynamic variables of the system. He defined the cavitation number (Cn) as

$$Cn = \frac{P_i - P_v}{P_i - P_{back}} \quad (1)$$

where $_{Pi}$, P_v, and P_{back} are the injection, saturated vapor pressure at the corresponding flow temperature, and back pressure, respectively. When the cavitation number is above the inception value, the flow is a single phase. The nucleus starts as Cn goes below the inception of cavitation. As the cavitation number decreases, vapor formation increases, leading to the formation of bubbles (inception), which transforms into a densely attached cavitation. Som et al.[14,15] noted that, in the presence of this phenomenon, bubbles that are in the case of growth will collapse due to the tensile stress on them. The collapse of the bubbles produces turbulent kinetic energy, which transfers to the liquid.[16] This energy is the main reason for the formation of vortices and disturbances leading to atomization. Yuan et al.[17] pointed out that cavitation in the nozzles has a strong effect on atomization and consequently the formation of downstream spray.

Studies on diesel fuel[18] indicated that the liquid outside the nozzle under the influence of cavitation has a droplet Sauter mean diameter (SMD) smaller than that of the noncavitating liquid. Since SMD indicates the quality of a spray atomization process,[19] the smaller the SMD, the finer the spray droplets, which means the better atomized spray. Other studies[20,21] showed that the breakup length of liquid jet with cavitation inside the nozzle is less and the spray cone angle is wider than their counterparts of noncavitating flow. This is attributed to the breakup of cavitation bubbles, which reinforce the turbulence at the nozzle exit.[22] Also, it is observed that the growth of cavitation volume inside the nozzle increases the jet speed at the nozzle exit.[23] This further stimulates the effect of aerodynamic forces leading to more atomization.

The behavior of the flow in and out of the atomizer nozzle has been investigated by many researchers.[24−26] They concluded that the Rayleigh−Plesset equation is well applied for all nuclei and bubbles tracked in a Lagrangian manner for the incipient cavitation regime. The bubbles are formed where the vorticity is evident. Chen et al.[27] studied the effect of temperature on the cavitation phenomena when methanol is used as the working fluid. The formation and condensation of the bubbles were solved by the Rayleigh−Plesset equation. They found that the cavitation density increases with the increase in methanol temperature. Han et al.[28] predicated the internal and external flows through various nozzle aspect ratios. The bubble dynamics were treated using the Rayleigh−Plesset equation. The study concluded that the locations within the nozzle, where cavitation is generated and collapse change with the change in length of atomizer nozzle.

A previous study shows that most of the ongoing work focus on the flow inside the nozzle, the flow at the nozzle, or the

https://doi.org/10.1021/acsomega.1c04272
ACS Omega 2021, 6, 33498−33510

issuing flow, which takes the form of the spray. They focused on correlating the aggregated phenomena on spray configurations. Yet there is a lack of computation approach to interlink these aggregated phenomena. The present paper presents a numerical simulation for the impact of in-nozzle flow on cavitation and consequently spray characteristic. This model is experimentally guided and verified using detailed experimental measurements. The effect and intensity of the cavitation on spray configurations have been experimentally investigated by the aid of a synchronized high-speed camera with a pulsated laser sheet, which has been used as a light source. Distilled water was used as a working fluid. To accelerate the presence of cavitation under the used injection pressure (10 bar), the water is heated to temperatures between 110 and 140 °C. The experimental results are used to guide and verify the computational model. Since the in- and out-nozzle flows are representing two different flow regimes, two models have been developed to simulate the two regimes. The first model considers the flow characteristics inside the injection nozzle considering the bubbly two-phase flow due to cavitation formation, while the second model considers spray characteristics outside the injection nozzle. A novel coupling formulation is used to develop the injection probability density function, to interlink the two models based on the analogy between turbulence and acoustic effect of the issuing jet from the inject nozzle. Using the verified model, the effect of the nozzle length (L)/diameter (D_n) of the nozzle is evaluated to investigate its impact on the locations of cavitation formation and collapse, as well as the effect of such impact on the issuing spray characteristics. Furthermore, the effect of nozzle geometrical features and operating conditions has been investigated.

2. EXPERIMENTAL SETUP AND MEASURING TECHNIQUES

A test rig, with a setup for controlled injection pressure and the temperature of the injected liquid, was designed to study the effect of in-flow nozzle on spray characteristics. Transparent single-hole nozzles made of glass are used to monitor and conduct necessary measurements for the continuously injected liquid. The hole diameter of all nozzle is 0.35 mm. The injection pressure is adjusted to 10 bar. To accelerate the inception of cavitation at the injection pressure of 10 bar, the injected water is heated to different temperature levels from 110 to 140 °C.

Figure 1 shows the schematic of the test rig, where the injection pressure and temperature of the injected liquid are controlled. Two measuring techniques are used to study the rate of generation of cavitation bubbles inside the nozzle hole and to evaluate the spray characteristics. These measuring techniques are nonintrusive laser-based techniques. They include particle sizing using the shadowgraph technique to visualize both the bubbles and the droplets of the cavitation inside the transparent glass nozzle and the spray outside the nozzle, respectively. Figures 2 and 3 depict the particle image velocimetry (PIV) technique that is used to measure the instantaneous planar velocity fields of the spray and its cone angle as well as cavitation bubbles imaging, respectively.

The cavitation bubbles generated inside the 0.35 mm nozzle is measured using shadowgraph technique. Full data about cavitation bubbles in every image like the number of bubbles, bubble diameter, and volume are obtained. As shown in Figure 5C, the bubbles do not always have a spherical shape, so the

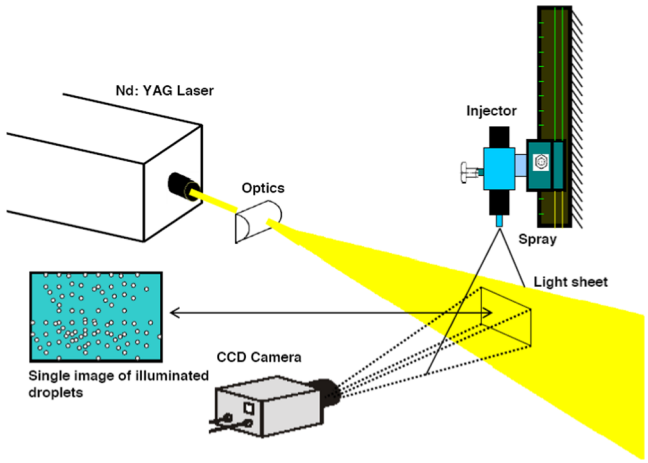

Figure 2. Schematic description of the experimental setup for PIV measurements.

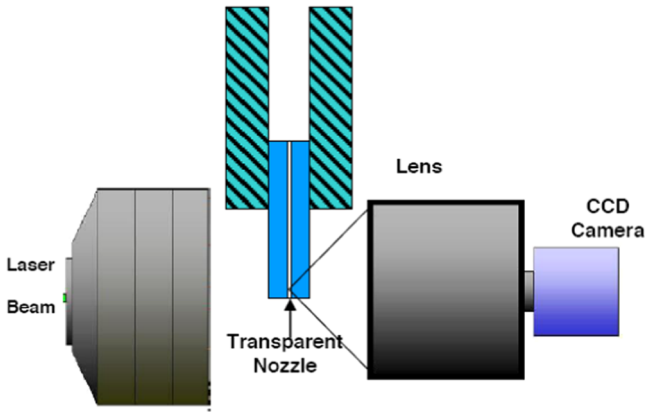

Figure 3. Measurement setup for cavitation bubbles generated inside the nozzle hole.

equivalent diameter for every bubble is measured by drawing different lines passing through the boundary of the bubble. Afterward, the mean length of these lines is taken as the equivalent bubble diameter. The ensemble mean volume of cavitation bubbles is calculated as the summation of the volumes of all bubbles, in all images, divided by the number of images that contain these bubbles, as follows

$$\text{ensemble mean volume of bubbles} = \frac{\text{total volume of bubbles in all images}}{\text{number of images}} \quad (2)$$

In the present study, 64 consecutive images are taken at every selected injection temperature.

The PIV velocity measurements reported in the present work are the ensemble mean of 20 realizations, since average values (mean and root mean square (RMS)) showed good convergence for at least 10 realizations. Twenty instantaneous velocity distributions are measured at each vertical cross section passing through the axis of the spray under the specified operating conditions. The ensemble mean velocity at each point on the grid $\bar{V}(x, y)$ was obtained using the following expression

$$\bar{V}(x, y) = \frac{\sum_i^N V_i(x, y)}{N} \quad (3)$$

https://doi.org/10.1021/acsomega.1c04272
ACS Omega 2021, 6, 33498−33510

where $\bar{V}(x, y)$ is the instantaneous velocity at the (x, y) grid node in the ith realization and N is the total number of realizations.

The geometry package software called "Single Line Spray Angle"[29] is used for spray cone angle detection. The algorithm starts at the defined injector position and examines each horizontal pixel line down to the bottom of the image. In this model, a single pixel line is taken to find the borders of the spray. The diameters of the spray together with the distance to the injector define the resulting spray cone angle. After calculation, the detected spray cone angle is drawn into the source image as overlay graphics, as shown in Figure 4.

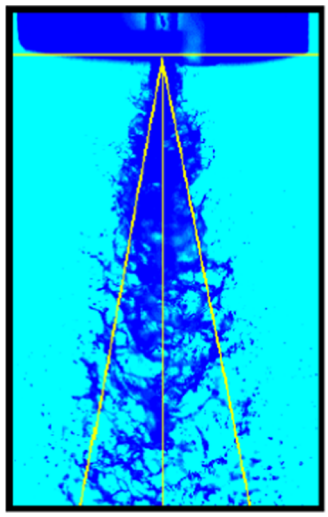

Figure 4. Spray cone angle measurement.

Different measurement positions with different magnifications were carried out, as shown in Figure 5. The overall measurement domain is shown in Figure 5A. Figure 5B shows the magnification plane of 10 mm × 12 mm, which is used to measure the intact column and the spray cone angle. This magnification is achieved using an extension tube of 25 mm length, which is fixed between the camera and camera lenses. Figure 5C shows the magnification plane of 0.5 mm × 0.6 mm to measure the cavitation bubble generation inside the nozzle hole. This magnification is done using an extension tube of 500 mm length, which is fixed between the camera and camera lenses. Figure 5D shows the measurement position to measure the collapse of the cavitation bubbles just before the exit of the nozzle. It uses the same magnification as in position (C). Finally, Figure 5E shows measurement inside the spray at an axial distance of 40 mm from the tip of the nozzle to measure the SMD of the spray droplets. It uses the same magnification as position (C).

3. DESCRIPTION OF THE COMPUTATIONAL MODEL

The mathematical model used for predicting the flow inside and outside of the nozzle hole is according to the previously developed work by the authors,[2] as illustrated in S1 (Appendix-A). It predicts the influence of the inflow on the outflow from the nozzle hole. The model is based on the phenomenological description of the flow, which has been concluded from the experimental observations.

Although both the in and out flows of the nozzle are two-phase flows; however, there is a significant difference between the two flows. As for the inflow, it starts as a single-phase liquid flow; then, it may be subjected to cavitation so that it turns into a bubbly flow. These bubbles may continue to grow, agglomerate, and transform into an annulus or a slug flow, or they may collapse and transform back into a highly turbulent monophasic flow. This is influenced by the flow characteristics and geometry of the flow passage. On the other hand, the outflow from the nozzle can be turned into spray, if cavitation is experienced inside the nozzle. Aerodynamic forces have an effect on this flow, which enhances its disintegration. This effect is emphasized when the flow speed is high such that the aerodynamic forces are stimulated. Accordingly, the outflow undergoes disintegration, leading to the formation of spray. The flow can be described as two phases, where the continuous phase is the gas and the dispersed phase constitutes the liquid droplets. The resulting spray goes through several stages from thick spray to diluted spray. Therefore, it is necessary to introduce coupling mechanisms between the two phases. These mechanisms include flow−droplet, droplet−flow, and droplet−droplet interactions.

Based on the aforementioned phenomenological description, the problem has been classified as three-dimensional, two-phase turbulent, and isothermal flow (where no droplet evaporation is taking place). Accordingly, the system of governing equations consists of the continuity and momentum equations (no energy equation has been considered, as the problem is considered isothermal). Suitable source terms, which interlink between the governing equations, have been identified. Several submodels are used to complement the simulation. These include turbulence modeling using the large eddy simulation (LES) approach as well as other models for the interaction between the two flow phases. These submodels are adjusted for both the in and outflows.

The system of governing equations solved using the finite difference technique is considered in the ANSYS-FLUENT-code. The nature of flow consists of a spectrum of eddy size ranging from the Kolmogorov length scale, at which the energy dissipation takes place, to the large eddies, which is the average flow. Based on the previous specification, the considered models and their submodels are illustrated, as shown in Figure 6.

As shown in Figure 6 for the in-flow model, the continuity and momentum equations of the mixture flow and phase change are simulated to predict the bubble formation. The rate of evaporation and condensation represent the bubble growth and collapse, which is according to the bubble dynamic equation "Rayleigh−Plesset equation". No slip between the two phases of the flow is considered. With regard to the turbulence simulation, large eddy simulation (LES) modeling has been considered to study the transport and confounding of different scales. For LES, large scales are solved directly. On the other hand, small turbulent scales are modeled. The spatial scale is differentiated by applying a low-pass filter to the governing equations. This set of filtered equations controls the dynamics of large scales. Spatial fluctuations, less than the specified filter cutoff length, are resolved using the subgrid model. In this study, the cutoff length is taken as the mesh size, which equals Taylor length scale. The spatial filtering process of a stream variable is defined as a function of time and space through the convolution integral.

Regarding the out-flow model, the issuing flow from the nozzle disintegrates to form the spray. This is due to the effect of the experienced cavitation inside the nozzle as well as the

https://doi.org/10.1021/acsomega.1c04272
ACS Omega 2021, 6, 33498−33510

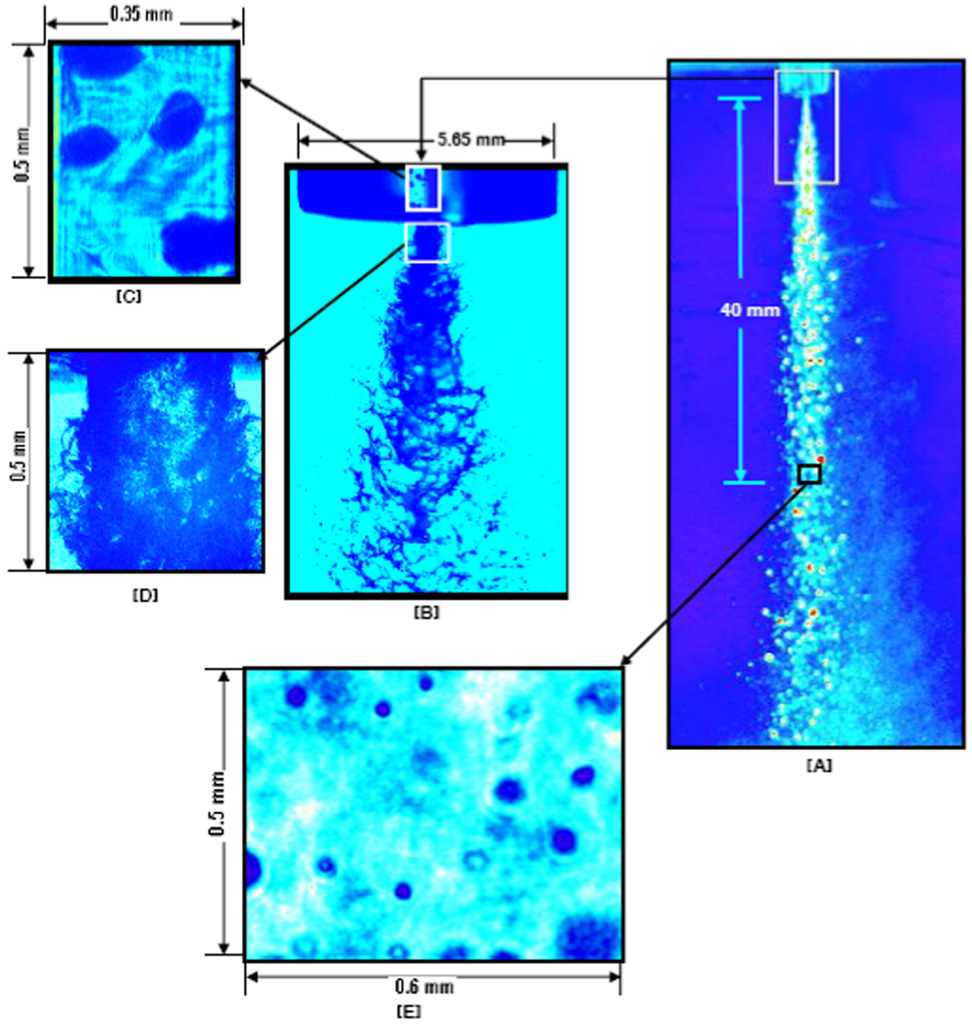

Figure 5. Different measurement positions with different magnifications.

effect of the aerodynamic forces, as a result of the high velocity of the issuing flow. According to the probability density function, the diameters and velocities of spray droplets are randomly determined. This probability density function takes the form of Rosin Rammler distribution function. The spray is modeled using the discrete drop model (DDM), where defined numbers of parcels are considered to represent the droplets. These representative parcels travel through the continuous gaseous phase. Using the Lagrangian formula, which includes hydrodynamic drag, inertia, and gravitational forces, the trajectories of the droplets are calculated. Both droplet collision and breakup models are considered. The discrete random walk model for the random effect of turbulence on droplet diffusion is taken into account.[30] Droplet breakup and collision models are included. These include the TAB model for droplet breakup as well as the droplet collisions model, which are developed by O'Rorke.[30] These models have been considered in the Fluent software.[30]

The state of the flow issuing from the nozzle and the effective area of the injection nozzle are key parameters in determining the spectrum of droplet size, velocity, and spatial distributions. This is greatly influenced by the cavitation density near the exit of the nozzle. When these cavitation bubbles collapse, turbulent kinetic energy is released to the flow. To determine the effect of the increase in the turbulent kinetic energy on the breakup of the issuing liquid jet into droplets and to find out the droplet size distribution, an analogy with ultrasonic atomizers is considered. The probability density function (PDF) of the injected flow is assumed to follow Rosin Rammler distribution. The mean diameter can be found out based on the surface tension, density, flow turbulent frequency, and the subgrid turbulent kinetic energy, as shown in eq S34 in the Supporting Information. The initial maximum droplet size is assumed to be equivalent to the value of the large vortices or orifice diameter. On the other hand, the minimum droplet size is taken equal to the Taylor length scale. These are calculated according to eqs S35 and S36, respectively, as shown in the Supporting Information.

The droplet velocity is defined based on the injection velocity, the effective nozzle area, and the mass flow rate generated by the flow model at the nozzle exit area. The trajectories of the droplets are randomly distributed such that they do not exceed the spray cone angle (θ). Considering the experimental results for the spray cone angle for a nozzle experiencing an in-flow cavitation, a correlation for the spray cone angle (θ) has been correlated as follows

$$\theta = (Cn)^a \left(\frac{L}{D_n}\right)^b \left(\frac{\rho_g}{\rho_l}\right)^c \left(\frac{k}{0.5\overline{u}^2}\right)^d \quad (4)$$

https://doi.org/10.1021/acsomega.1c04272
ACS Omega 2021, 6, 33498−33510

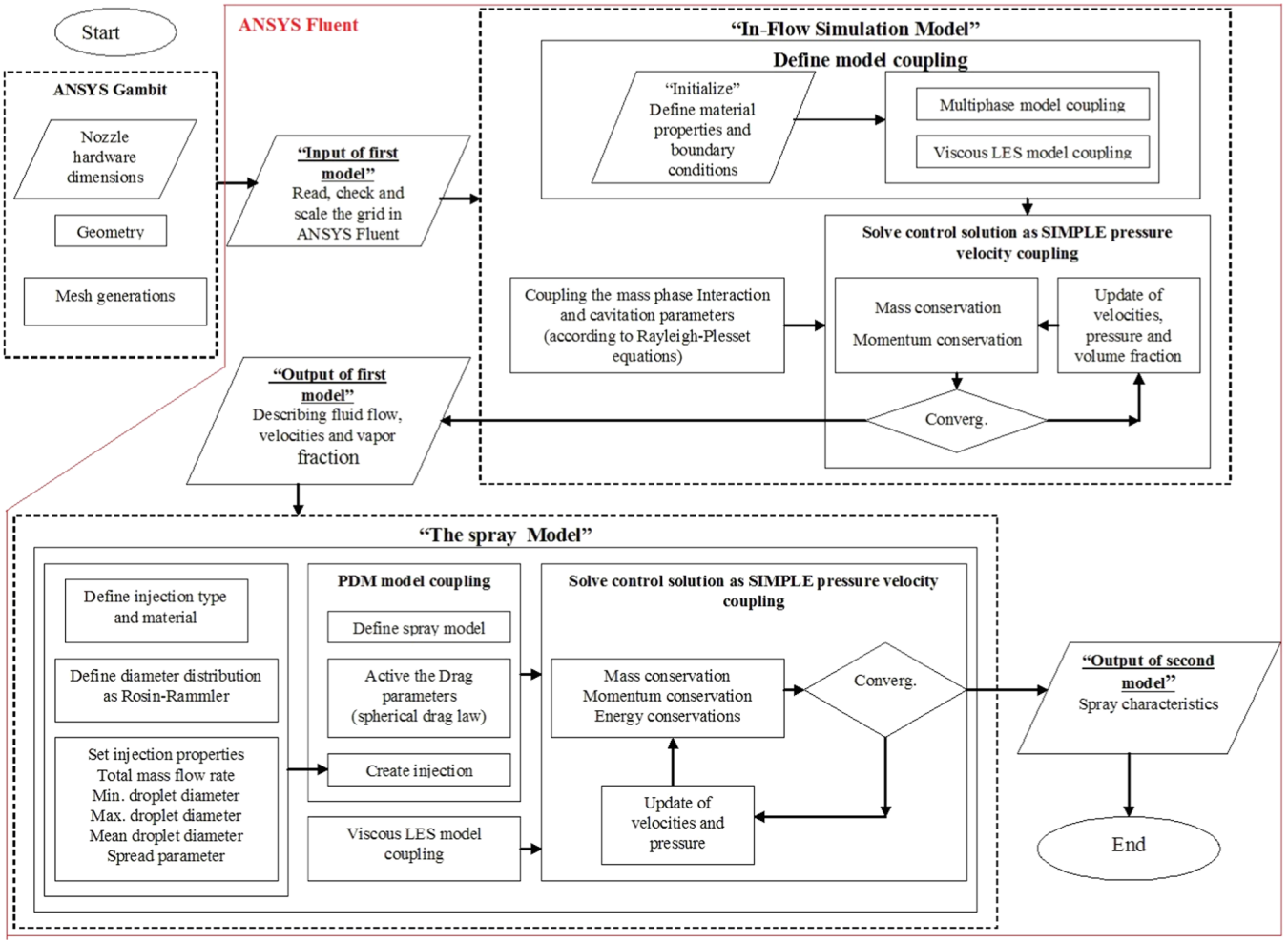

Figure 6. Models considered and their submodels.

where

$$a = 17.4236,\ b = 14.0682,\ c = 8.1761,\ d = 0.3458$$

Regarding the boundary conditions, they are defined as shown in Table 1.

Table 1. Types of the Boundary Conditions

boundary conditions	the zone
pressure inlet	inlet
no slip	wall
pressure outlet	outlet

Since a turbulence model is used, the mesh is intensified at the wall to show the effect of velocity gradient due to the presence of the wall.

4. ASSESSMENT OF COMPUTATIONAL ACCURACY

The computational accuracy and stability are affected by the grid size and time step, respectively. The size of the grid cells has been taken to be equal to Taylor microscale. The Taylor microscale is inertial subrange, which falls in between the large-scale eddies (containing the energy range) and the small-scale eddies or Kolmogorov length scale (dissipation range). This scale size of the grid can capture the small eddy scales. The most critical value of the solution is the volume vapor fraction at 1.5 mm before the exit of the nozzle. As shown in the results, this indicator has an impact on the released turbulent kinetic energy, which leads to the disintegration of the liquid into droplet.

A grid sensitivity analysis is carried out based on the values of the parameters considered in the experimental work to find the change in the volume vapor fraction at 1.5 mm before the exit of the nozzle. It has been taken as an indicator for the impact of the grid size on the accuracy of the solution, considering different grid sizes. Three grid sizes are considered in this analysis. The different grid sizes are controlled by eq 5 and shown in Table 2.

$$Ri_x = \frac{\Delta X_{\text{coarse}}}{\Delta X_{\text{medium}}} = \frac{\Delta X_{\text{medium}}}{\Delta X_{\text{fine}}} = 2 \tag{5}$$

The order of convergence p is calculated from the least-squares fit of the data.[31,32] Accordingly, the Richardson extrapolation[31,32] is applied using the two finest grids to obtain an estimate of the value of the volume fraction at zero grid spacing, Y_{ref}. The Richardson extrapolation provides an

Table 2. Grid/Solution Sensitivity

mesh type	grid spacing (ΔX)	volume fraction (Y)
fine	0.01	0.0800
medium	0.02	0.0794
coarse	0.04	0.0768

https://doi.org/10.1021/acsomega.1c04272
ACS Omega 2021, 6, 33498−33510

estimation of the solution due to eq 6, as shown in Table 3. Accordingly, the percentage error "e" in the solution relative to

Table 3. Result of Richardson Extrapolation

Richardson extrapolation	calculated value	eq no.
$P \approx \frac{\ln[\frac{Y(\Delta X_{medium}) - Y(\Delta X_{coarse})}{Y(\Delta X_{fine}) - Y(\Delta X_{medium})}]}{\ln(Ri_x)}$	= 2.115	(6)
$Y_{ref} \approx \frac{Ri_x{}^P \times Y(\Delta X_{fine}) - Y(\Delta X_{medium})}{Ri_x{}^P - 1}$	= 0.0802	(7)
$e_{coarse} = \frac{(Y_{ref} - Y(\Delta X_{coarse}))}{Y_{ref}}$	= 0.0422	(8)
$e_{medium} = \frac{(Y_{ref} - Y(\Delta X_{medium}))}{Y_{ref}}$	= 0.0097	(9)
$e_{fine} = \frac{(Y_{ref} - Y(\Delta X_{fine}))}{Y_{ref}}$	= 0.0022	(10)

the Richardson extrapolation can be calculated for the different grid sizes for the coarse, medium, and fine grids, as calculated by eqs 8−10, respectively, as shown in Table 3.

Considering and acceptable error of 0.22% for the fine grid. The fine grid is considered for the proposed numerical solution. This grid has grid quality with a maximum cell squish of 0, maximum aspect ratio of 6.6, and skewness of 0.4. Regarding the time step (Δt) impact on the solution accuracy, increasing the time step will increase the truncation errors introduced in the approximation process.

On the other hand, selecting a very small time step should be avoided since in addition to the high computational time required for a solution, the accuracy of the solution will be dominated by round-off errors.[33] Stability analysis indicates that the solution is stable when the diffusion number (dn) should be less than or equal to (1/2).[33] The time step can be calculated according to the following equation

$$dn = \frac{\upsilon \Delta t}{(\Delta x)^2} + \frac{\upsilon \Delta t}{(\Delta y)^2} + \frac{\upsilon \Delta t}{(\Delta z)^2} \quad (11)$$

where Δx, Δy, and Δz are the minimum space step in respective directions and υ is the kinematic viscosity in (m^2/s).

5. RESULTS AND DISCUSSION

A cylindrical single-hole nozzle is used as the base case. The nozzle continuously injects heated distilled water into the free

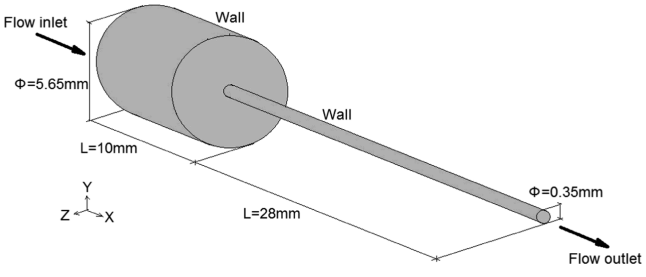

Figure 7. Schematic drawing of single-hole nozzle.

atmosphere. Figure 7 shows the geometrical configuration of the nozzle. The nozzle has an inlet diameter of 5.65 mm at the supply side, an outlet diameter of 0.35 mm at the exit of the nozzle, and a length of 28 mm. Accordingly, the nozzle has (L/D_n) = 80 and Cn = 0.81 (equivalent to the liquid temperature of 130 °C), as shown in Figure 8, for the relation between the cavitation number and liquid temperature. Based on the

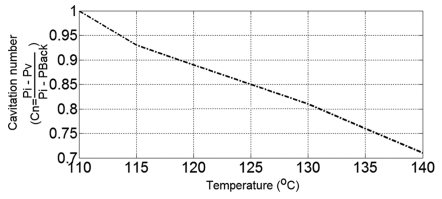

Figure 8. Effect of temperature on cavitation number.

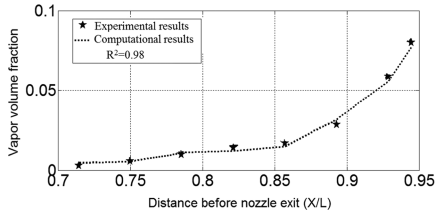

Figure 9. Vapor volume fraction along the nozzle hole axis at Cn = 81 (equivalent to the liquid temperature of 130 °C).

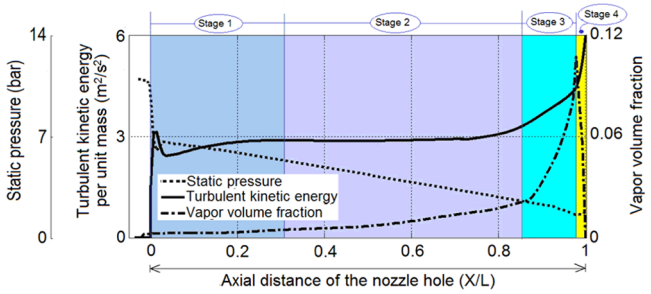

Figure 10. Change of static pressure, turbulent kinetic energy, and vapor volume fraction along the axial distance of the nozzle hole (Cn = 0.81).

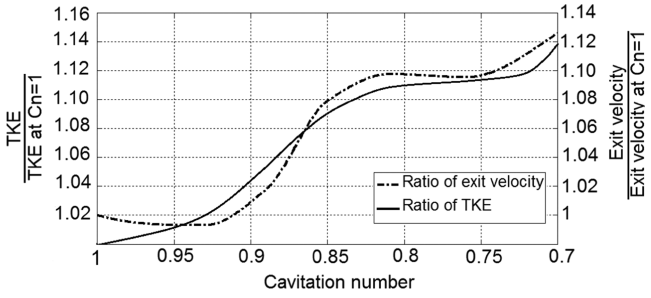

Figure 11. Effect of cavitation number on exit velocity and turbulence kinetic energy.

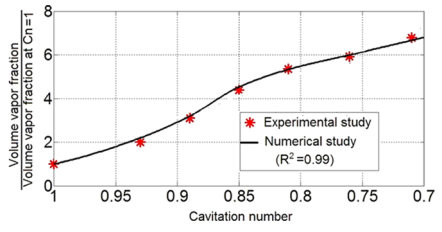

Figure 12. Evolution of the ratio of vapor volume fraction to a reference vapor volume fraction at Cn = 1 as a result of decrease in the cavitation number.

https://doi.org/10.1021/acsomega.1c04272
ACS Omega 2021, 6, 33498−33510

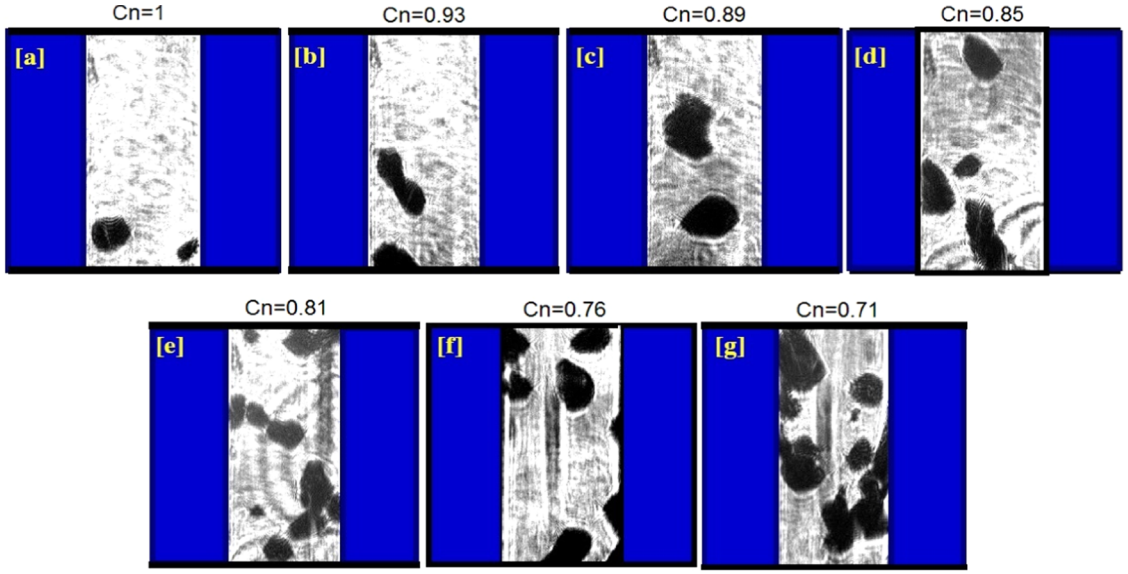

Figure 13. Samples of images showing the bubble generation at different cavitation numbers: (a) *Cn* = 1, (b) *Cn* = 0.93, (c) *Cn* = 0.89, (d) *Cn=0.85*, (e) *Cn* = 0.81, (f) *Cn* = 0.76, and (g) *Cn* = 0.71.

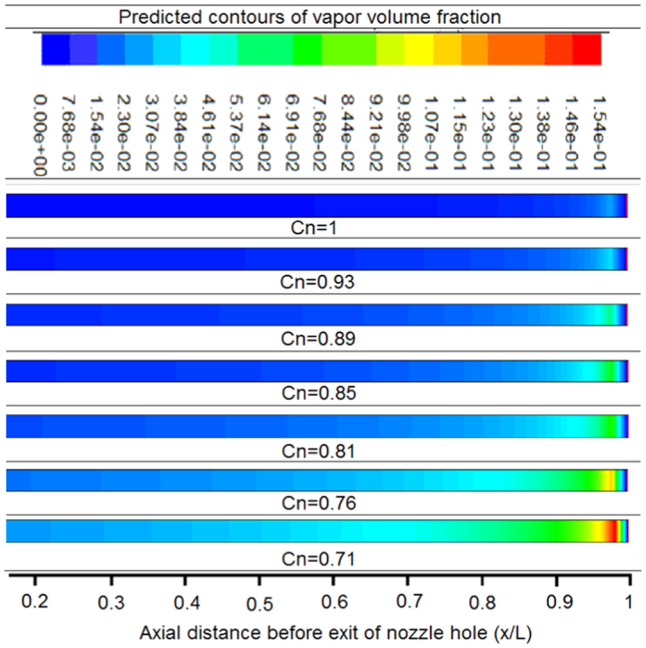

Figure 14. Effect of cavitation number on vapor volume fraction inside single-nozzle holes.

experimental observations, as distilled water is injected from the upstream to the downstream, the pressure decreases down to the vaporization pressure corresponding to the liquid temperature. This reduction in the pressure causes the formation of cavitation bubbles, which grow from the position of formation toward the direction to the exit of the nozzle. Close to the nozzle exit, bubbles collapse as a result of the back pressure.

Figure 9 shows a comparison between the experimental and the corresponding computational results for the volume fraction. As shown in the figure, the R^2 value is predicted to be 0.98 compared with the experimental results.

According to the experimental observations and the corresponding predictions, the development of turbulent kinetic energy and vapor volume fraction of the injected water passes through four stages, as shown in Figure 10. In the first stage, which starts from the entrance of the nozzle to X/L equals 0, the axial flow is restricted and retarded by the effect of the nozzle wall. This leads to the increase in the core velocity to satisfy the incompressible continuity. Due to the generated shear layers, turbulent kinetic energy increases quickly and the vapor starts to form. The latter is attributed to the friction and vortices, which leads to the dissipation of the turbulent energy, near the wall. A sharp decrease in static pressure contributes to the production of cavitation. The occurrence of eddies can result in small-size ligaments. This provides the necessary energy for the formation of nuclei, which leads to the occurrence of microbubbles. Continuing moving downstream the second stage can be identified. It extends from X/L = 0.30 to X/L = 0.85. In this stage, the boundary layers merge, leading to a fully developed flow. Both turbulent kinetic energy and vapor volume fraction increase gradually. The microbubbles generated in the previous stage travel through this stage with little growth. This was followed by a third stage, where the rate of increase in vapor volume fraction becomes steeper, the bubble size increases, and their radii approach a critical value. This stage covers the range from X/L = 0.85 to X/L = 0.97. This change in phase generates fluctuations, which enhances the turbulent kinetic energy. Besides, the generated bubbles may choke the flow. At the fourth stage, which extends from X/L = 0.97 to the exit of the nozzle, the effect of the back pressure at the exit of the nozzle causes bubble collapse. The collapsed bubbles near the exit of the nozzle substantially enhance the turbulent kinetic energy, leading to the disintegration of the discharged jet.

Figure 11 shows the relation between the turbulent kinetic energy at the exit of the nozzle and the flow cavitation number. As shown in the figure, the turbulent kinetic energy at the exit of the nozzle increases as the cavitation number becomes less. This is attributed to the increase in cavitation with the reduction of the cavitation number such that the liquid flow becomes more bubbly, turning it into a two-phase flow. As the bubbly flow approaches the nozzle exit and due to the resistance at the nozzle exit, pressure increases, leading to the

https://doi.org/10.1021/acsomega.1c04272
ACS Omega 2021, 6, 33498−33510

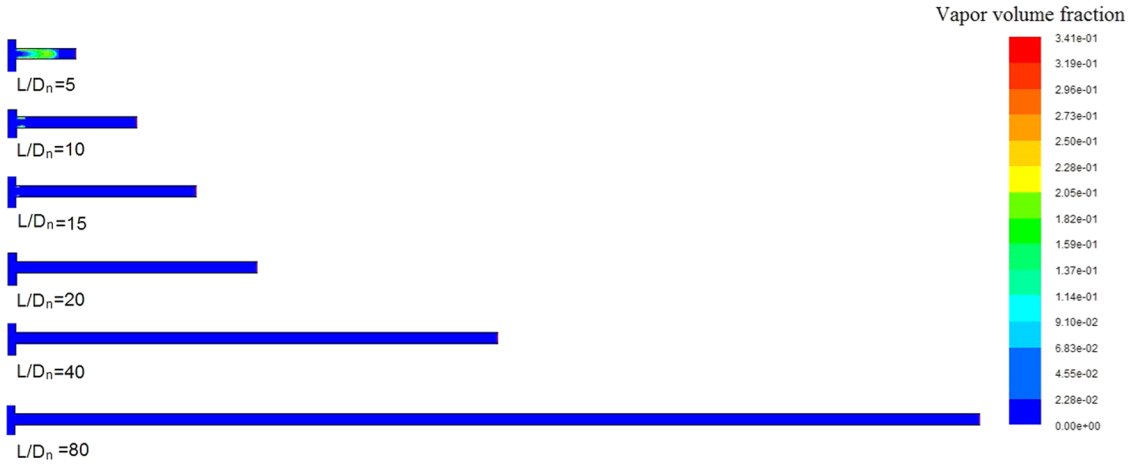

(a) $T=25^{o}C$ and $Cn>1$

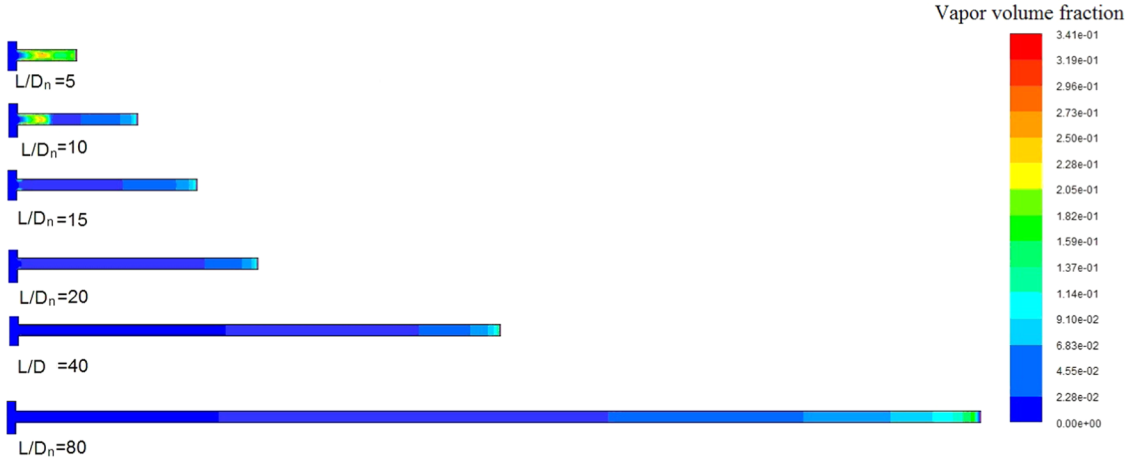

(b) T=130°C and $Cn=0.81$

Figure 15. Cavitation location as a function of nozzle (L/D_n) at different temperatures and cavitation number values.

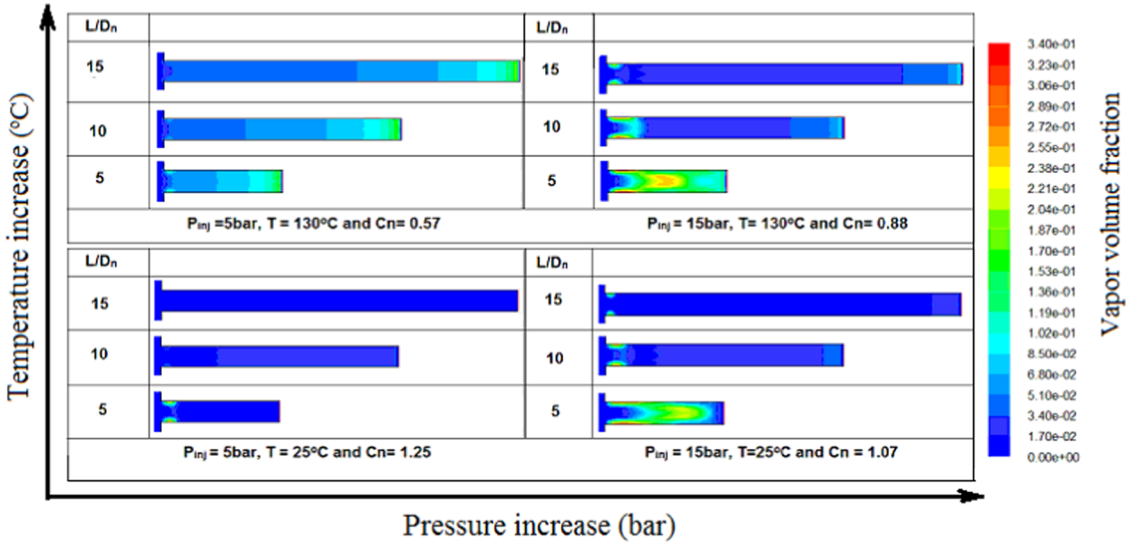

Figure 16. Cavitation location as a function of injection pressure and temperature.

collapse of the bubbles. This enhances the flow turbulent kinetic energy, where it reaches its maximum value just at the exit. As a result, the frequency and fluctuation increase and spread downstream to the exit of the nozzle. This mechanism is the main factor for the primary breakup of the liquid jet into droplets.

https://doi.org/10.1021/acsomega.1c04272
ACS Omega 2021, 6, 33498−33510

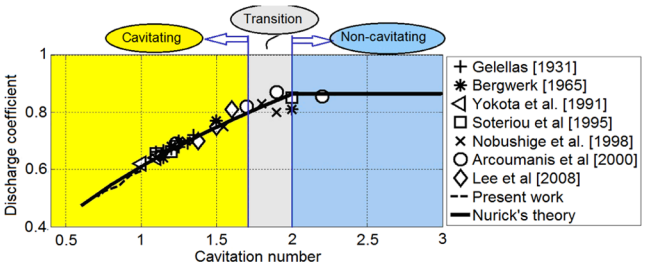

Figure 17. Comparison of the present work with Nurick's theory and other experimental studies.

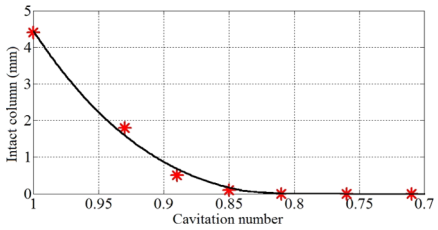

Figure 18. Effect of cavitation bubbles generated inside the nozzle hole on the length of spray intact column.

Figure 12 shows a linear relation, which exists between the cavitation number and vapor volume fraction inside the nozzle at distance X/L = 0.95 before the nozzle exit. When the cavitation number is 30% less compared with Cn = 1, the ratio of volume fraction increases by approximately 8 times. Figure 13 visually confirms these results, which illustrates that the captured images from the experiment for the cavitation bubble, when the cavitation number changes from 1 to 0.71. It shows that the vapor volume fraction near the nozzle exit increases with the reduction in the cavitation number. This is consistent with the computational results. A good agreement can be found between the results of the computational model and the experimental work with R^2 = 0.99, as shown in Figure 12.

Figure 14 shows the contours of vapor volume fraction generated inside the nozzle with the variation of the injected water temperature. This is consistent with the experimental measurements, as shown in Figure 13 at X/L= 0.8 to X/L = 0.98. As cavitation occurs, vapor volume fraction reaches its highest value at a distance between X/L = 0.95 and 0.97 before the nozzle exit. For the cases of lower cavitation number, this area extends backward. This means that as the temperature increases and consequently the cavitation number decreases, cavitation occurs earlier before the nozzle exit.

The impact of the length-to-diameter ratio (L/D_n) of the injection nozzle on the location and intensity of the cavitation inside the nozzle is assessed. Four aspect ratios of 80, 40, 20, and 10 are considered in this assessment. Considering the cases of liquid temperatures of 25 and 130 °C, the predictions indicate that the cavitation location, intensity, and extension are affected by the aspect ratio and liquid temperature, as shown in Figure 15. Figure 15a shows the cavitation location at a temperature of 25 °C with different aspect ratios. As shown in the figure, cavitation is observed with a strong intensity when the nozzle has a small aspect ratio. Cavitation starts at the entrance and extends toward the exit direction of flow. The cavitation intensity decreases with the increase in the aspect ratio. It disappears when the aspect ratio is above 20. These results are consistent with those observed by Han et al.[28]

Figure 15b shows the increase in cavitation when the temperature of the liquid is 130 °C. As shown in the figure, cavitation occurs near the entrance of the nozzle due to the sudden contraction, where the vorticity is formed. This happens when L/D_n is small. Cavitation disappears near the entrance as L/D_n increases. Cavitation moves close to the exit of the nozzle, which is attributed to the formation of homogeneous vapor nuclei within the flow, when its pressure decreases near the exit of the nozzle. This result is consistent with the case studied experimentally.

As shown in Figure 16, the pressure and temperature of the injected liquid as well as the geometrical characteristics of the injector affect the formation and locations of the cavitation inside the nozzle. As shown in the figure, this can take three alternative forms; the first is when pressure increases, while the liquid temperature is ambient. In this case, the cavitation is formed at the entry of the nozzle and extends in the direction of the flow. Yet, for longer (L/D_n), the cavitation shrinks back toward the injection nozzle entry. The second case is when the temperature of the injected liquid increases while the injection pressure is kept constant. In this case, the cavitation appears closer to the exit of the nozzle. As (L/D_n) increases, the cavitation becomes closer to the nozzle exit. Regarding the third alternative in case both the pressure and temperature increase, cavitation appears larger at the entry area and extends toward the exit. As the (L/D_n) of the nozzle increases, cavitation is formed at both entry and exit. However, cavitation close to the exit has less intensity compared with that at the entry.

According to the aforementioned analysis, it can be concluded that injection pressure and liquid temperature are dynamic drivers for the place of the onset of cavitation and its extension inside the injection nozzle. However, pressure is considered more effective. On the other hand, geometry of the nozzle is a key factor affecting the shape and locations of the cavitation inside the nozzle.

Injection pressure is another factor that controls the cavitation phenomena. As shown in Figure 16, as the injection pressure increases, for the case of Cn higher than 1, the transitional (L/D_n) from cavitated flow to noncavitated flow is becoming higher. On the other hand, when Cn is less than 1, cavitation occurs anyway, regardless of the value of injection pressure.

The exit flow velocity depends directly on the effective cross-sectional area of the nozzle. The presence of bubbles, as a result of cavitation, affects the net cross-sectional flow area, where bubbles occupy the internal area of the cross section and reduce the area of fluid passage through this section. This increases the liquid flow velocity, as shown in Figure 11. This velocity further increases as the cavitation number of the liquid becomes less. The liquid flow velocity at the nozzle exit increases by 12.5%, as the cavitation number decreases from 1 to 0.70, as a result of bubble growth. The bubbles collapse when they approach the exit of the nozzle. The energy generated from the collapse delivers more forces leading to the acceleration of the issuing flow from the nozzle. This further enhances the aerodynamic forces on the emerging jet, leading to the atomization and increase of the spray volume.

To extend the verification of the computational model, the obtained numerical results are compared with reported experimental results for the discharge coefficient developed by other researchers, under different operating conditions. Figure 17 depicts the relation between the ranges of the

https://doi.org/10.1021/acsomega.1c04272
ACS Omega 2021, 6, 33498−33510

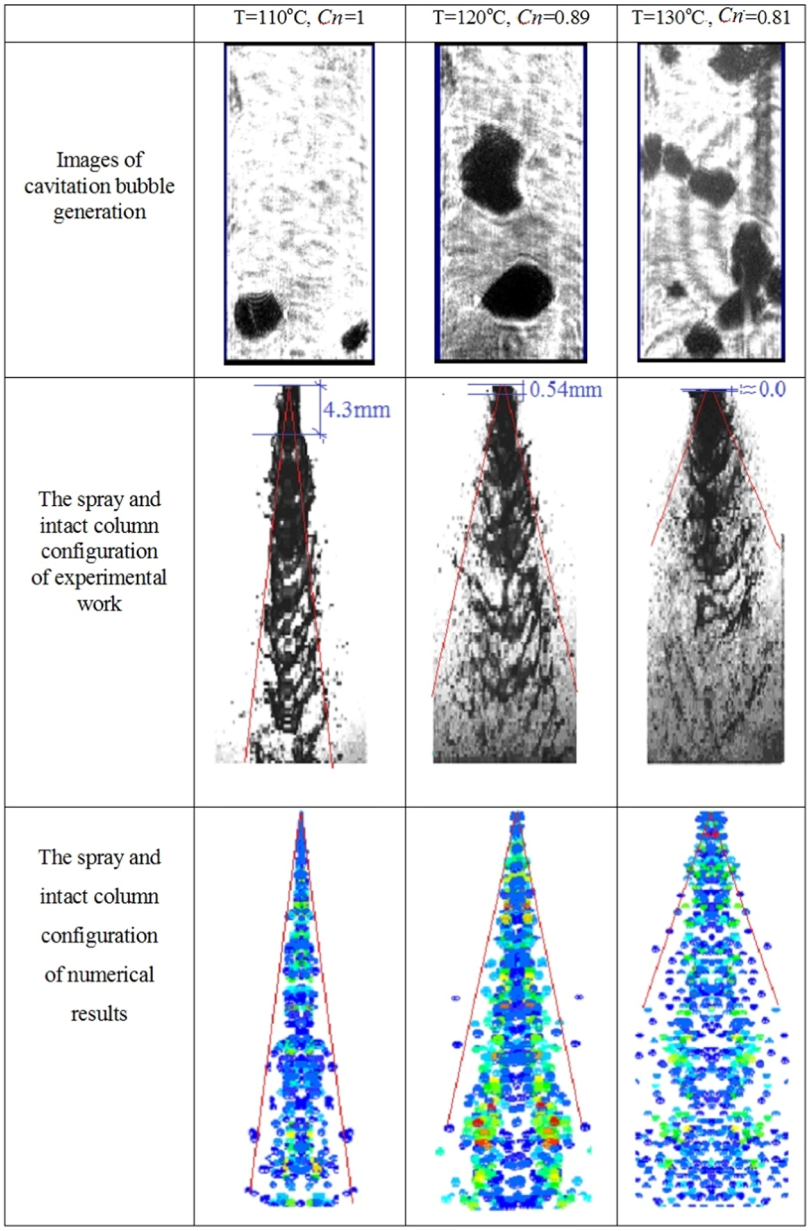

Figure 19. Effect of cavitation bubbles generated inside the nozzle hole on spray intact column.

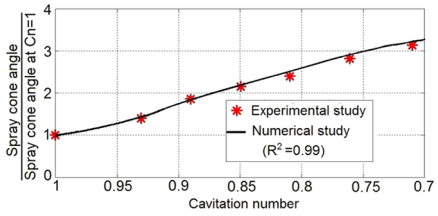

Figure 20. Relation between the cavitation number and the spray cone angle.

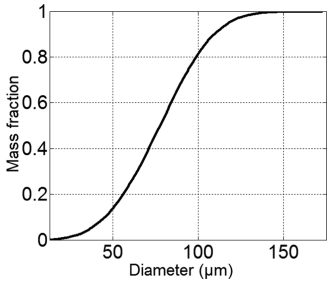

Figure 21. Developed PDF for spray atomization.

cavitation numbers and discharge coefficient, as predicted by the computational model, against different experimental results developed by other researchers as well as Nurick's theory.[34] According to Nurick's theory, the discharge coefficient is directly proportional to the square root of cavitation number. This follows Nurick correlation ($C_d = C_c\sqrt{Cn}$), where C_d is the discharge coefficient and C_c is the contraction coefficient. As shown in the figure, a very good agreement can be found between the experimental work for different operating conditions and nozzle configurations and the developed model.

Figure 18 shows that the intact column decreases with a decrease in the cavitation number. When the cavitation bubbles start to form at Cn = 1, the intact column reaches

https://doi.org/10.1021/acsomega.1c04272
ACS Omega 2021, 6, 33498−33510

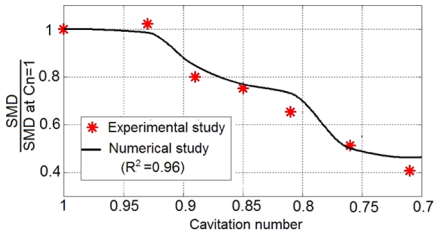

Figure 22. Relation between the cavitation number and the cross-section-averaged SMD at a distance of 40 mm from the nozzle outlet.

4.3 mm. Beyond this intact column, the spray begins to have a small divergence. At this cavitation number, a small number of cavitation bubbles are generated, leading to the breakup of the stable jet into a large number of long ligaments. Outside the nozzle, the bubbles collapse because of the ambient pressure, which is above the vapor pressure of the water. This collapse disturbs the jet. When the rate of cavitation bubble generated inside the nozzle increases, the ligaments are broken up and the intact column becomes shorter. It becomes 0.54 mm as the cavitation number reaches 0.89. The intact column disappears as the cavitation number decreases, and the visible ligaments at the nozzle exit decrease until they completely break up into small droplets at Cn = 0.81. At this value of Cn, the cavitation bubbles generated inside the nozzle increase and the finest atomization is observed.

The effect of cavitation bubbles generated inside the nozzle hole, by heating the injected water, on the spray cone angle is shown in Figure 19. Once the cavitation begins within the nozzle hole, there is a small divergence of the jet at the hole exit and the spray is clearly atomizing at the exit. There is a tendency for the spray cone angle to increase as the injected water temperature increases. Outside the nozzle, the bubble collapse disturbs the jet and the formed droplets become more widely distributed. This effect leads to a pronounced increase in the spray cone angle. Figure 20 shows that the spray cone angle increases as the cavitation number decreases. Considering the experimental and computational results, the relation is nearly linear, where the ratio of spray cone angle increases by about 35−40% when the cavitation number decreases by about 0.05.

To have a closure for the solution, a coupling between the in and out flows of the nozzle is needed. The probability density function (PDF) represents the coupling equation, which describes the initial transformation from a liquid column to droplets. It has been defined through the identification of three values for the droplet's diameters. These include the maximum, mean, and minimum droplet sizes. The initial maximum droplet size is assumed to be equivalent to the value of the large vortices or orifice diameter. The mean droplet is defined based on the impact of the turbulence intensity of droplet atomization, which developed through the analogy with the impact of the ultrasonic waves on the liquid column for atomization, as in the case of ultrasonic atomizers. This is explained in Section 3. Equations S33−S36 in the Supporting Information show the development and definitions of the Sauter mean, maximum, and minimum diameters of the injected droplet probability density function. Regarding the minimum droplet size, it is taken to be equal to the Taylor length scale. The three values are fitted using Rosin Rammler distribution. The developed probability density function is shown in Figure 21.

The change in the SMD of the spray droplets accompanying the changes in cavitation number is shown in Figure 22. This figure is obtained by processing the corresponding images of the spray droplets taken at an axial distance of 40 mm from the tip of the atomization nozzle, using a magnification plane of 0.5 mm × 0.6 mm and the particle sizing using the shadowgraph technique. Also, the characteristics of the liquid spray and atomization at a position 40 mm away from the nozzle exit are determined by experimental work. The decrease in SMD is shown both numerically and experimentally when Cn decreases. An agreement can be seen between the numerical and experimental results (R^2 = 0.96). These results confirm the validity of the predicted probability density function for the initial droplet distribution considering the analogy between the turbulence generation due to the collapse of the cavitation bubbles inside the injection nozzle and acoustic atomization.

6. CONCLUSIONS

Cavitation is the main influencing phenomenon for the primary atomization of liquid in pressure atomizers. The characteristics of the cavitation inside the injection nozzle including its location, length, and volume fraction depend on the values of the cavitation number Cn, geometrical characteristics of the nozzle, and operating conditions. The experimental results have been successfully simulated computationally, and a very good agreement between the simulations and the experimental results has been found, where the "R^2" value for the regression analysis is very close to 1 (0.98−0.99). The validation process for the inflow model has been extended to include additional experimental results developed by other researchers that are obtained under different nozzle configurations and operating conditions. The validity of the predicted probability density function for the initial droplet distribution considering the analogy between the turbulence generation due to the collapse of the cavitation bubbles inside the injection nozzle and acoustic atomization has been confirmed through the agreement between the predicted droplet size and the corresponding measurements in the developed spray. Regarding nozzle geometrical configurations, the ratio of the nozzle length to its diameter is a key factor affecting the shape and locations of the cavitation inside the nozzle and consequently spray configuration. Regarding operating conditions, both liquid injection pressure and temperature are dynamic drivers for the onset of cavitation and its extension inside the injection nozzle, yet pressure is more effective.

■ ASSOCIATED CONTENT

Supporting Information

The Supporting Information is available free of charge at https://pubs.acs.org/doi/10.1021/acsomega.1c04272.

Mathematical model used for predicting the flow inside and outside of the nozzle hole illustrated in Appendix (PDF)

■ AUTHOR INFORMATION

Corresponding Author

Mahmoud Abd El-Aziz Mohamed − *Department of Mechanical Power Engineering, Faculty of Engineering, Zagazig University, Sharkia 4419, Egypt;* orcid.org/0000-0003-2386-1084; Email: eng.mah1981@yahoo.com

https://doi.org/10.1021/acsomega.1c04272
ACS Omega 2021, 6, 33498−33510

Authors

Hesham El-Sayed Abdel Hameed − *Department of Mechanical Power Engineering, Faculty of Engineering, Zagazig University, Sharkia 4419, Egypt*

ElShenawy A. ElShenawy − *Department of Mechanical Power Engineering, Faculty of Engineering, Tanta University, Gharbiya 31527, Egypt*

Hafez Abdel Aal El-Salmawy − *Department of Mechanical Power Engineering, Faculty of Engineering, Zagazig University, Sharkia 4419, Egypt*

Ramy Elsayed Shaltout − *Department of Mechanical Power Engineering, Faculty of Engineering, Zagazig University, Sharkia 4419, Egypt*

Complete contact information is available at: https://pubs.acs.org/10.1021/acsomega.1c04272

Notes

The authors declare no competing financial interest.

REFERENCES

(1) Bayvel, L.; Orzechowski, Z. *Liquid Atomization*; Routledge, 2019.

(2) Mohamed, M. A. E.-A.; Abdel Hameed, H. E.; Shaltout, R. E.; El-Salmawy, H. A. A. Prediction of the Impact of Nozzle Geometry on Spray Characteristics. *ACS Omega* **2021**, *6*, 6218−6230.

(3) Alidoost Dafsari, R.; Lee, H.; Han, J.; Lee, J. Evaluation of the Atomization Characteristics of Aviation Fuels with Different Viscosities Using a Pressure Swirl Atomizer. *Int. J. Heat Mass Transfer* **2019**, *145*, No. 118704.

(4) Payri, R.; Salvador, F. J.; Gimeno, J.; De la Morena, J. Analysis of Diesel Spray Atomization by Means of a near-Nozzle Field Visualization Technique. *Atomization Sprays* **2011**, *21*, 753−774.

(5) Tanasawa, Y.; Toyoda, S. A Study on the Atomization of High Speed Liquid Jets (1st Report). *Trans. Jpn. Soc. Mech. Eng.* **1954**, *20*, 299−306.

(6) Charalampous, G.; Hardalupas, Y. How Do Liquid Fuel Physical Properties Affect Liquid Jet Development in Atomisers? *Phys. Fluids* **2016**, *28*, No. 102106.

(7) Rokhsar Talabazar, F.; Jafarpour, M.; Zuvin, M.; Chen, H.; Gevari, M. T.; Villanueva, L. G.; Grishenkov, D.; Koşar, A.; Ghorbani, M. Design and Fabrication of a Vigorous "cavitation-on-a-Chip" Device with a Multiple Microchannel Configuration. *Microsyst. Nanoeng.* **2021**, *7*, No. 44.

(8) Liu, X.; Wu, Z.; Li, B.; Zhao, J.; He, J.; Li, W.; Zhang, C.; Xie, F. Influence of Inlet Pressure on Cavitation Characteristics in Regulating Valve. *Eng. Appl. Comput. Fluid Mech.* **2020**, *14*, 299−310.

(9) Balz, R.; Nagy, I. G.; Weisser, G.; Sedarsky, D. Experimental and Numerical Investigation of Cavitation in Marine Diesel Injectors. *Int. J. Heat Mass Transfer* **2021**, *169*, No. 120933.

(10) Hiroyasu, H. Spray Breakup Mechanism from the Hole-Type Nozzle and Its Applications. *Atomization Sprays* **2000**, *10*, 511−527.

(11) Joseph, D. D. Cavitation and the State of Stress in a Flowing Liquid. *J. Fluid Mech.* **1998**, *366*, 367−378.

(12) Movaghar, A. *The One-Dimensional Turbulence Model Applied to Spray Atomization*; Chalmers Tekniska Hogskola: Sweden, 2018.

(13) Nurick, W. H. Orifice Cavitation and Its Effect on Spray Mixing. *J. Fluids Eng.* **1976**, *98*, 681−687.

(14) Som, S.; Aggarwal, S. K.; El-Hannouny, E. M.; Longman, D. E. Investigation of Nozzle Flow and Cavitation Characteristics in a Diesel Injector. *J. Eng. Gas Turbines Power* **2010**, *132*, No. 042802.

(15) Som, S.; Douglas, E.; Anita, I.; Aggarwal, S. Influence of Nozzle Orifice Geometry and Fuel Properties on Flow and Cavitation Characteristics of a Diesel Injector. In *Fuel Injection in Automotive Engineering*; Lejda, K., Ed.; InTech, 2012.

(16) Vejražka, J.; Zedníková, M.; Stanovsky, P. Experiments on Breakup of Bubbles in a Turbulent Flow. *AIChE J.* **2018**, *64*, 740−757.

(17) Yuan, W.; Schnerr, G. H. Numerical Simulation of Two-Phase Flow in Injection Nozzles: Interaction of Cavitation and External Jet Formation. *J. Fluids Eng.* **2003**, *125*, 963−969.

(18) Irannejad, A.; Jaberi, F. Numerical Study of High Speed Evaporating Sprays. *Int. J. Multiphase Flow* **2015**, *70*, 58−76.

(19) Chen, L.; Liu, Z.; Sun, P.; Huo, W. Formulation of a Fuel Spray SMD Model at Atmospheric Pressure Using Design of Experiments (DoE). *Fuel* **2015**, *153*, 355−360.

(20) Payri, F.; Payri, R.; Salvador, F. J.; Martínez-López, J. A Contribution to the Understanding of Cavitation Effects in Diesel Injector Nozzles through a Combined Experimental and Computational Investigation. *Comput. Fluids* **2012**, *58*, 88−101.

(21) Yang, S.; Wang, S.; Sun, Z.; Li, X.; Hung, D. L. S.; Xu, M. In-Nozzle Bubble Formation and Its Effect on Fuel Jet Breakup under Cavitating and Flash Boiling Conditions. *Appl. Therm. Eng.* **2021**, *183*, No. 116120.

(22) Song, Y.; Wang, D.; Yin, J. lian.; Li, J.; Cai, K. Experimental Studies on Bubble Breakup Mechanism in a Venturi Bubble Generator. *Ann. Nucl. Energy* **2019**, *130*, 259−270.

(23) Li, X.; Yang, S.; Li, T.; Hung, D. L. S.; Xu, M. Investigations on near-Field Atomization of Flash Boiling Sprays for Gasoline Direct Injection Related Applications. *Fuel* **2019**, *257*, No. 116097.

(24) Mlkvik, M.; Stahle, P.; Gauke, V.; Karbstein, H.; Jedelsky, J.; Jicha, M. Twin-Fluid Atomization of Viscous Liquids: The Effect of Atomizer Construction on Breakup Process, Spray Stability and Droplet Size. *Int. J. Multiphase Flow* **2015**, *77*, 19−31.

(25) Laurila, E.; Koivisto, S.; Kankkunen, A.; Saari, K.; Maakala, V.; Järvinen, M.; Vuorinen, V. Computational and Experimental Investigation of a Swirl Nozzle for Viscous Fluids. *Int. J. Multiphase Flow* **2020**, *128*, No. 103278.

(26) Dober, G.; Shi, J.-M.; Guerrassi, N.; Karimi, K.; Meslem, Y. *Complex Physics Modelling of Diesel Injector Nozzle Flow and Spray Supported by New Experiments*; 2014.

(27) Chen, Z.; Yao, A.; Yao, C.; Yin, Z.; Xu, H.; Geng, P.; Dou, Z.; Hu, J.; Wu, T.; Ma, M. Effect of Fuel Temperature on the Methanol Spray and Nozzle Internal Flow. *Appl. Therm. Eng.* **2017**, *114*, 673−684.

(28) Han, D.-S.; Lee, B.; Chang, Y.-J.; Song, J.-H.; Jeon, C.-H. *A Numerical Study of Spray Characteristcs through Various Nozzle Aspect Ratio*, ILAss: Italy, 2008.

(29) LaVision GmbH. *Product-Manual for DaVis 8.1*. LaVision GmbH: Anna-Vandenhoeck-Ring 19, D-37081 Göttingen, 2013.

(30) Fluent Inc. *Fluent User's Guide*, 2009.

(31) Hemez, F. M. In *Numerical Uncertainty in Computational Engineering and Physics*. 2nd International Conference on Uncertainty in Structural Dynamics, Sheffield, U.K., June 15, 2009.

(32) Carrillo, V. M.; Petrie, J. E.; Pacheco, E. A. Application of the Grid Convergence Index to a Laminar Axisymmetric Sudden Expansion Flow. *Maskana* **2014**, *5*, 115−123.

(33) Hoffmann, K. A.; Chiang, S. T. *Computational Fluid Dynamics for Engineers*; Engineering Education System: Wichita, KS, 1993.

(34) Rakshit, S. High Speed Flow Simulation in Fuel Injector Nozzles. Ph.D. Thesis, University of Massachusetts Amherst, 2012.